Thin Solid Films 571 (2014) 260–267

Contents lists available at ScienceDirect

Thin Solid Films

journal homepage: www.elsevier.com/locate/tsf

Effect of layer thickness on the high temperature mechanical properties of Al/SiC nanolaminates

S. Lotfian [a], C. Mayer [b], N. Chawla [b], J. Llorca [a,c], A. Misra [d], J.K. Baldwin [d], J.M. Molina-Aldareguía [a,*]

[a] IMDEA Materials Institute, c/Eric Kandel 2, 28906 Getafe, Madrid, Spain
[b] Materials Science and Engineering, Arizona State University, Tempe, AZ 85287-6106, USA
[c] Department of Materials Science, Polytechnic University of Madrid, E.T.S. de Ingenieros de Caminos, 28040 Madrid, Spain
[d] Los Alamos National Laboratory, Los Alamos, NM 87545, USA

ARTICLE INFO

Available online 18 June 2014

Keywords:
Metal–ceramic composite
Multilayers
Layer thickness
Nanolaminate
High temperature nanomechanics
Nanoindentation

ABSTRACT

Composite laminates on the nanoscale have shown superior hardness and toughness, but little is known about their high temperature behavior. The mechanical properties (elastic modulus and hardness) were measured as a function of temperature by means of nanoindentation in Al/SiC nanolaminates, a model metal–ceramic nanolaminate fabricated by physical vapor deposition. The influence of the Al and SiC volume fraction and layer thicknesses was determined between room temperature and 150 °C and, the deformation modes were analyzed by transmission electron microscopy, using a focused ion beam to prepare cross-sections through selected indents. It was found that ambient temperature deformation was controlled by the plastic flow of the Al layers, constrained by the SiC, and the elastic bending of the SiC layers. The reduction in hardness with temperature showed evidence of the development of interface-mediated deformation mechanisms, which led to a clear influence of layer thickness on the hardness.

1. Introduction

Natural and synthetic composite laminates have demonstrated an excellent combination of strength and toughness [1]. Nanoscale multilayer or nanolaminates constitute a special case, when the layer thicknesses are reduced <100 nm. Nanolaminates in different combinations (metal–metal [2–5], metal–ceramic [6–9], and ceramic–ceramic [10–13]) have typically shown unique electrical [14], magnetic [15–17], optical [18,19], and mechanical properties [20,21], as a consequence of the nanoscale dimensions of the layers and/or the large interfacial area. Designing layered structures at nanoscale is therefore an attractive strategy for developing multifunctional materials to be used in different applications: wear resistant coatings, optical coatings for thermosolar energy generation, supercapacitors and/or electrical interconnects. Even in the latter examples, mechanical performance is crucial, because nanolaminate coatings will be often subjected to high stresses and temperatures under operation conditions. However, there is very little information available on the mechanical properties at high temperature of thin-films because of the experimental difficulties to carry out high temperature nanoindentation.

Progress in instrumented nanoindentation has opened the possibility to carry out nanoindentation and micropillar compression tests at high temperature [22–25] and these techniques were recently used to study the mechanical properties of Al/SiC nanolaminates, a model metal–ceramic nanolaminate. Previous work showed that Al/SiC nanolaminates with Al and SiC layer thicknesses of 50 nm presented very high room temperature strength [7,26–31], as a result of the constraint imposed by the stiff SiC layers on the plastic deformation of the Al nanolayers. However, the strength dropped quickly with temperature as a result of the large reduction in yield stress with temperature experienced by the Al nanolayers and the onset of interfacial sliding between layers [30,31], at least for equal thicknesses of the elastic SiC and plastic Al layers.

Following this line of research, this investigation was focused on the effect of temperature on the elastic modulus and hardness of Al/SiC nanolaminates as a function of the relative layer thicknesses of Al and SiC. To this end, nanolaminates with Al and SiC layer thicknesses in the range 2 to 100 nm were manufactured by magnetron sputtering and their Young's modulus and hardness were measured between 28 °C and 150 °C. The nanoindentation imprints were cross-sectioned using a focused ion beam (FIB) and analyzed by transmission electron microscopy (TEM) to ascertain the deformation modes as a function of layer thickness and temperature.

2. Materials and experimental procedure

The nanolaminates were fabricated by magnetron sputtering alternating layers of Al and SiC onto a single crystal silicon wafer (111).

* Corresponding author.
E-mail address: jon.molina@imdea.org (J.M. Molina-Aldareguía).

http://dx.doi.org/10.1016/j.tsf.2014.06.022
0040-6090/

The sputter unit is made up of high vacuum chamber with dual sputter guns. Targets of pure Al (99.99%) and SiC (99.5%) (Kurt J. Lesker, Clairton, PA) were used for sputtering in Ar atmosphere at a working pressure of 3.0 mTorr (0.4 Pa). Al was sputtered using a DC sputter gun with a power of 95 W and SiC layers were deposited using identical argon pressure and an RF sputter power of 215 W. The targets were pre-sputtered for 10 min at 40 W for Al and 95 W for SiC to remove any oxides and contaminates prior to film deposition. With these conditions, the deposition rates were 7.5 nm min^{-1} for Al and 3.9 nm min^{-1} for SiC. The sample holder was continuously rotated during sputtering to obtain uniform layer thicknesses. The individual layer thicknesses were varied between 2 and 100 nm, and the total numbers of layers were selected to ensure total film thicknesses above 10 μm. The large total film thickness ensured negligible substrate effects during indentation testing. In order to investigate the effect of the individual layer thickness on the mechanical response, two series of samples were produced (see Table 1). In series 1, the SiC layer thickness was kept constant at 50 nm while the Al layer thickness varied between 10 and 100 nm; in series 2, the Al layer thickness was kept constant at 50 nm while the SiC layer thickness varied between 2 and 100 nm. The nanolaminates were named by their Al and SiC nominal layer thicknesses in nanometers, e.g. Al10SiC50 refers to a nanolaminate containing 10 nm thick Al layers and 50 nm thick SiC layers. The last column in Table 1 indicates the volume fraction of Al in each nanolaminate, according to the nominal layer thicknesses.

Nanoindentation tests were carried out using a NanoTest™ platform III (Micro Materials, Wrexham, UK) with a Berkovich diamond tip. Nanoindentation testing was performed at 28 °C, 50 °C, 100 °C, and 150 °C. Samples were bonded to the heater plate using a high temperature adhesive and then both, sample and indenter were heated independently to the target temperature. Independent heating of tip and sample is the best way to control thermal drift, so that drift rates lower than 0.01 nm s^{-1} can be achieved prior to testing. Indentations were carried out with a loading rate of 10 mN s^{-1} up to a maximum load of 100 mN. The maximum load was held constant for a dwell period of 5 s at maximum load prior to unloading at 20 mN s^{-1}. The creep rate was computed in all cases at the end of the hold period and it was always below 0.1 nm s^{-1}, ensuring negligible creep effects on the determination of the elastic modulus from the unloading stiffness. Upon unloading, thermal drift was measured again by introducing a 60-second hold segment at 10% of the maximum load. The drift rate was measured over the last 40 s of the hold segment.

At least 8 indentations were performed at each temperature and the samples were kept at the test temperature for at least 3 h. The load–displacement curves were analyzed using the Oliver and Pharr method [32]. Selected indentations were characterized by atomic force microscopy (AFM), using a Park XE-150 instrument (Park Systems, Suwon, Korea) to carry out a more detailed analysis of the indentation contact area and to study pile-up/sink-in effects.

The microstructure of the nanolaminates was characterized using a dual beam FIB (FEI, Nova 200 NanoLab). To ascertain the deformation modes, selected indentation imprints were cross-sectioned and observed by TEM, using a JEOL JEM 3000 microscope.

Table 1
Number of layers and layer thicknesses of the Al/SiC nanolaminates.

Series	Sample	Thickness (μm)	Number of layers	t_{Al} (nm)	t_{SiC} (nm)	V_{Al}
S1	Al10SiC50	15	250	10	50	0.17
	Al25SiC50	13.3	200	25	50	0.33
	Al50SiC50	14	150	50	50	0.50
	Al100SiC50	12	100	100	50	0.67
S2	Al50SiC2	12.8	289	50	2	0.96
	Al50SiC10	12.3	250	50	10	0.83
	Al50SiC25	13	200	50	25	0.67
	Al50SiC100	14	100	50	100	0.33

3. Results

3.1. Layer morphology

Representative TEM bright-field images of the cross-section of various nanolaminates are shown in Fig. 1. They include (a) Al50SiC50, (b) Al50SiC2, (c) Al50SiC10 and (d) Al10SiC50. The SiC layers were amorphous in all cases while the Al layers were nanocrystalline, with columnar grains whose average width (parallel to the layers) was of the order of 2–3 times the layer thickness. The interfaces between Al and SiC were chemically abrupt, with no evidence of chemical reactions, but physically rough as a result of the competitive columnar grain growth during deposition of each Al layer. The layer roughness was not large enough to break up the layered structure, even in the case of the Al50/SiC2 nanolaminate, where the SiC layers were only 2 nm thick (Fig. 1(b)). The actual layer thicknesses, as measured by TEM, compared well with the nominal layer thicknesses and were uniform through the entire thickness of each nanolaminate. All nanolaminates were apparently pore free, except for laminate Al10/SiC50, that showed evidence of porosity, presumably aligned along columnar grain boundaries, as indicated by the arrows in Fig. 1(d). This TEM image was recorded at slightly under focused conditions to reveal the Fresnel contrast associated with the pores.

3.2. High temperature nanoindentation

Representative load–indentation depth curves at room temperature of three different nanolaminates are plotted in Fig. 2. They correspond to, Al10SiC50, Al50SiC50 and Al50SiC10 and the Al volume fraction was 0.17, 0.50 and 0.83, respectively. As expected, the resistance to the indenter penetration decreased with the Al volume fraction due to the much higher hardness of SiC. The maximum indentation depth was always below 1200 nm and, therefore, within 10% of the total laminate thickness, which is a widely accepted rule-of-thumb to avoid substrate effects in the indentation response. Similar curves to those shown in Fig. 2 were analyzed using the Oliver and Pharr method [32] to compute the hardness and the elastic modulus of different nanolaminates. The Poisson's ratio of each nanolaminate was estimated as the average of the direct and the inverse rule of mixtures assuming that the Poisson's ratio of Al and SiC were 0.34 and 0.14, respectively [31,22,33]. The hardness and elastic modulus of all the nanolaminates are summarized in Table 2.

It is well known that the Oliver and Pharr method [32] may not provide accurate values of the hardness and elastic modulus if significant pile-up takes place around indentations. In order to confirm the applicability of the Oliver and Pharr method in these nanolaminates, the contact area was measured using AFM from the surface profile of indentation imprints in all samples at different temperatures. The topography results showed no significant pile-up around the indentations, as illustrated in Fig. 3 for selected indentations, confirming the accuracy of the data included in Table 2.

3.3. Deformation mechanisms

Fig. 4 shows an indentation cross-section in the Al50SiC10 nanolaminate. Remarkably, the layered structure was preserved in the deformed region and the strain imposed by the indenter was accommodated by the plastic deformation of the Al layers, plus the elastic deflection of the SiC layers. No dislocations could be found in the Al layers, but their thickness was reduced under the indented area, evidencing that they deformed plastically under the constraint of the stiff and hard SiC layers. It is also worth noting that the SiC layers underwent substantial bending under the indenter, because their small thickness allowed large elastic deformations without fracture. Nevertheless the SiC layers could not always accommodate the shear deformation imposed by the indenter, and were broken, as shown by the arrow in Fig. 4(b). Similar

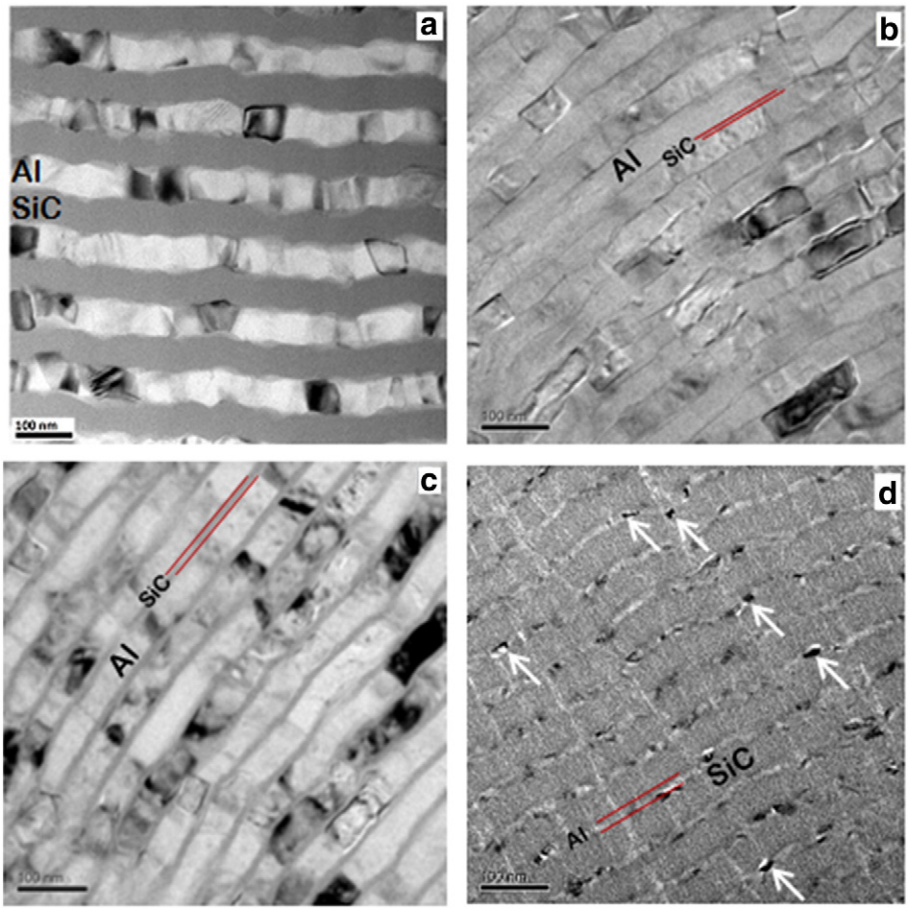

Fig. 1. TEM bright-field images of the cross-section of the various Al/SiC nanolaminates. (a) Al50SiC50, (b) Al50SiC2, (c) Al50SiC10, and (d) Al10SiC50. The arrows indicate pores.

observations in Al/SiC nanoscale multilayers [26,34,35], together with numerical simulations [28,31,36,37], have led to conclude that the high hardness of Al/SiC nanolaminates is a consequence of constrain imposed by the SiC layers to the plastic deformation of the Al layers.

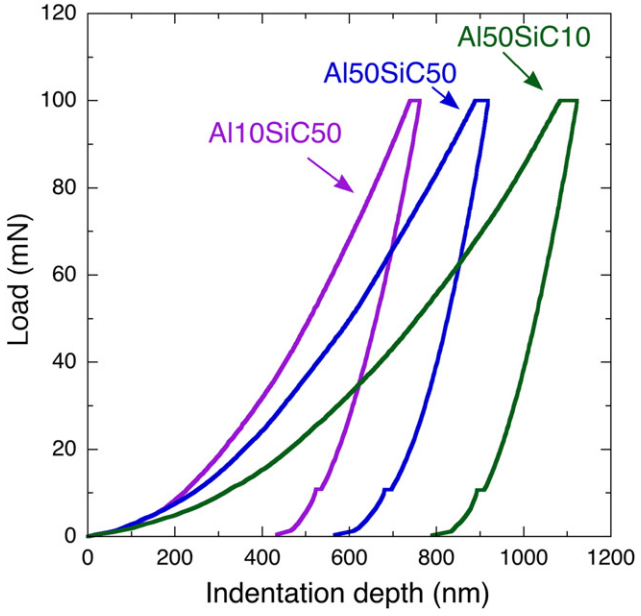

Fig. 2. Indentation load–displacement curves of Al–SiC nanolaminates with different layer thicknesses at room temperature.

TEM observations of the remaining nanolaminates, including those deformed at temperatures of up to 150 °C, were similar. Changes in the deformation and fracture mechanisms with layer thicknesses were not found, except in the nanolaminate Al50SiC2. In this particular case, the SiC layer thickness was so small, 2 nm, that the layered structure was apparently not preserved under the indenter (Fig. 5).

4. Discussion

4.1. Effect of layer thickness and temperature on the elastic modulus

The elastic moduli of both series of nanolaminates as a function of Al volume fraction are depicted in Fig. 6(a). The data clearly show that, as expected, the elastic modulus only depends on the volume fraction of the constituents and is independent of their individual layer thicknesses. For instance, Al25SiC50 and Al50SiC100 nanolaminates, both with an Al volume fraction of 0.33, present the same elastic modulus even though the layer thickness in the latter is twice that of the former. The same behavior was found in Al50SiC25 and Al100SiC50, both with an Al volume fraction of 0.67. This result was maintained at all temperatures between room temperature (RT) and 150 °C, as shown in Fig. 4(b) at 100 °C.

It is interesting to compare the elastic modulus of the nanolaminates with those of the constituents. The elastic modulus of Al and SiC monolithic coatings deposited under the same conditions were determined previously [38] as a function of temperature. While the elastic modulus of SiC was 300 GPa and increased slightly at 100 °C up to 320 GPa, the elastic modulus of Al decreased from 90 GPa at RT down to 70 GPa at 100 °C. Due to the layered structure, the nanolaminates are expected to display a very anisotropic behavior, with bounds given by the Voigt

Table 2
Elastic modulus and hardness of Al–SiC nanolaminates between 28 **°C** and 150 **°C**.

Sample	28 °C		50 °C		100 °C		150 °C	
	H (GPa)	*E* (GPa)	*H* (GPa)	*E* (GPa)	*H* (GPa)	*E* (GPa)	*H* (GPa)	*E* (GPa)
Al10/SiC50	9.7 ± 0.1	172 ± 1	9.2 ± 0.3	173 ± 5	7.4 ± 0.1	166 ± 4	6.1 ± 0.2	141 ± 2
Al25/SiC50	8.1 ± 0.5	161 ± 4	7.2 ± 0.2	153 ± 3	5.2 ± 0.1	141 ± 4	4.0 ± 0.1	149 ± 2
Al50/SiC50	5.7 ± 0.3	141 ± 3	5.3 ± 0.1	135 ± 1	3.9 ± 0.2	130 ± 3	3.1 ± 0.3	141 ± 7
Al100/SiC50	5.5 ± 0.4	127 ± 5	5.2 ± 0.4	122 ± 5	4.2 ± 0.3	116 ± 6	3.6 ± 0.2	116 ± 4
Al50/SiC2	3.3 ± 0.2	92 ± 4	2.8 ± 0.1	91 ± 1	1.5 ± 0.1	84 ± 6	1.2 ± 0.1	80 ± 8
Al50/SiC10	4.1 ± 0.1	105 ± 2	3.6 ± 0.2	101 ± 3	2.6 ± 0.1	104 ± 1	2.0 ± 0.1	106 ± 2
Al50/SiC25	4.8 ± 0.1	112.6 ± 2	4.4 ± 0.2	113 ± 3	3.5 ± 0.2	117 ± 4	2.7 ± 0.2	116 ± 5
Al50/SiC100	7.6 ± 0.3	152 ± 3	7.2 ± 0.3	144 ± 3	5.4 ± 0.1	135 ± 2	4.0 ± 0.2	140 ± 5

and Reuss averages. In the longitudinal direction, and assuming a perfect interface, Al and SiC deform under isostrain conditions, and therefore, the longitudinal nanolaminate elastic modulus will approach the Voigt average:

$$E_c = E_{Al}V_{Al} + E_{SiC}V_{SiC} \tag{1}$$

while the layers deform under isostress conditions in the transverse direction, and the elastic modulus approaches the Reuss average:

$$E_c = \frac{1}{\frac{V_{Al}}{E_{Al}} + \frac{V_{SiC}}{E_{SiC}}} \tag{2}$$

where *V* represents the volume fraction of each constituent, as indicated by the subscripts. The dotted and solid lines in Fig. 6(a) and (b) represent the Voigt and Reuss averages, respectively, as obtained by the elastic moduli of Al and SiC at each temperature. The agreement of the nanoindentation modulus with the Reuss average was excellent, particularly at room temperature, with the only exception of the Al10SiC50 nanolaminate, which was below the Reuss average at room temperature and 100 °C. This result can be explained by the intercolumnar porosity observed by TEM (Fig. 1(d)). The origin of this porosity is not clear but it could be the result of some problem during deposition.

The excellent agreement of the nanoindentation elastic modulus with the Reuss average was somewhat surprising. Even though the indentation loading direction is perpendicular to the layers, the stress field under the indenter is very complex, and substantial deformation is expected to take place both in the longitudinal and transverse directions. Therefore, the indentation modulus was expected to be somewhere between the Voigt and Reuss averages. In any case, the results are in good agreement with previous studies in Al/SiC nanolaminates with equal Al and SiC layer thicknesses [26]. Moreover, previous results

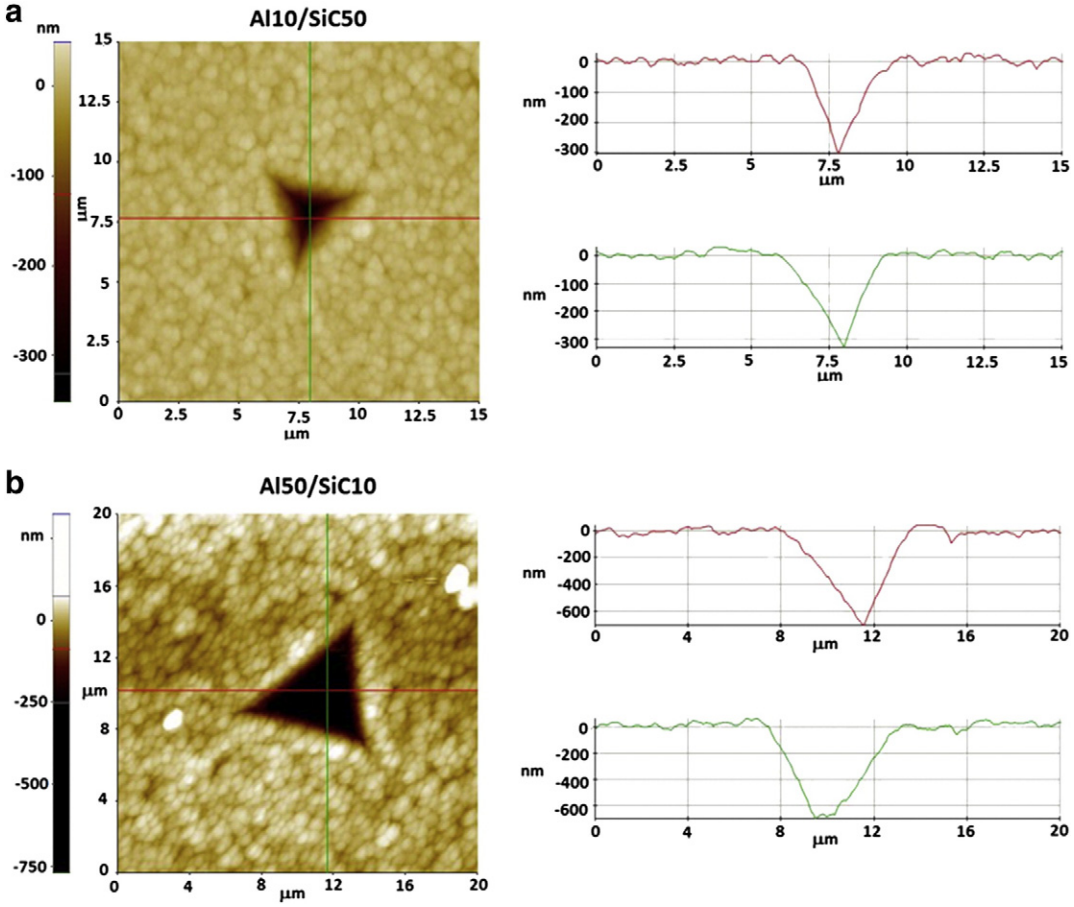

Fig. 3. AFM topography scans of residual indents of (a) Al10/SiC50 and (b) Al50/SiC10. No evidence of any significant pile-up was found.

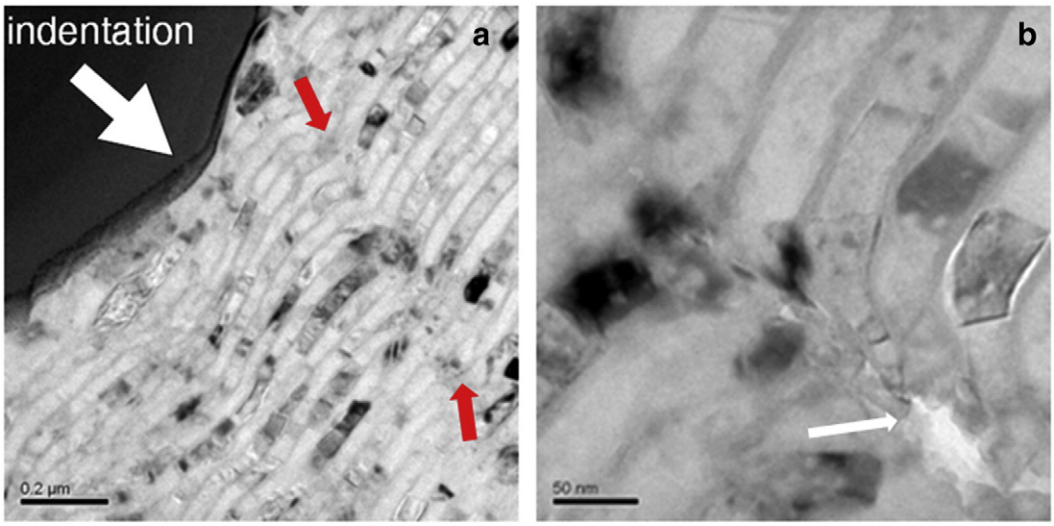

Fig. 4. Indentation cross-section in the Al50/SiC10 nanolaminate obtained by TEM: (a) general view, (b) detail of the fracture of SiC layers.

have demonstrated a good agreement between the elastic modulus determined by nanoindentation and by micropillar compression [26,31], with the former only being slightly larger than the latter, even though loading during micropillar compression is uniaxial and transverse to the layers. There might be two explanations for this. Firstly, even though the nanoindentation stress field is very complex, the major contribution to the elastic recovery takes place in the indentation direction [9]. As a matter of fact, it is well known that the projected area of the indentation imprint remains fairly constant and that only the depth is recovered during elastic unloading. Secondly, the assumption of a perfect interface may not be accurate. In fact, previous micropillar compression studies in Al/SiC nanolaminates up to 100 °C have demonstrated that substantial interface sliding might take place during deformation.

4.2. Effect of layer thickness and temperature on hardness

The evolution of the room temperature hardness with the Al volume fraction is plotted in Fig. 7(a) for both series of nanolaminates. The hardness of monolithic SiC and Al coatings was 30 GPa and 0.9 GPa, respectively. These results show that the hardness of the nanolaminates decreased more or less linearly as the Al volume fraction increased from 9.7 GPa for $V_{Al} = 16\%$ down to 3.3 GPa for $V_{Al} = 96\%$. As expected, the hardness of the nanolaminates was not given by some rule-of-mixtures of the hardness and volume fraction of the constituents but it did not depend on the layer thickness. This result was surprising because the hardness should be controlled by the dominant deformation mechanisms, which involve the elastic bending of SiC layers and the plastic deformation of Al constrained by the SiC layers. It is well established that the yield stress of the Al layers increases rapidly as the layer thickness decreases (following a potential law with a power exponent in the range -1 to -0.5), and thus it should be expected that – for a given volume fraction of Al – the nanolaminate with thinner Al layers should be stronger. However, since the indentation also involves substantial elastic bending of the SiC layers, thinner SiC layers might require lower loads to bend, because the flexural modulus of a plate scales with the cube of the plate thickness. Moreover, if interface sliding is also taking place during deformation, the area fraction of interfaces (which is inversely proportional to the layer thickness) should also play a role. Therefore, the surprising observation described in Fig. 7(a) showing that, in the range of layer thicknesses studied, the room temperature hardness is determined by the volume fraction of the constituents might be due to the fact that upon the reduction of layer thickness, the increase in the yield stress of Al is compensated

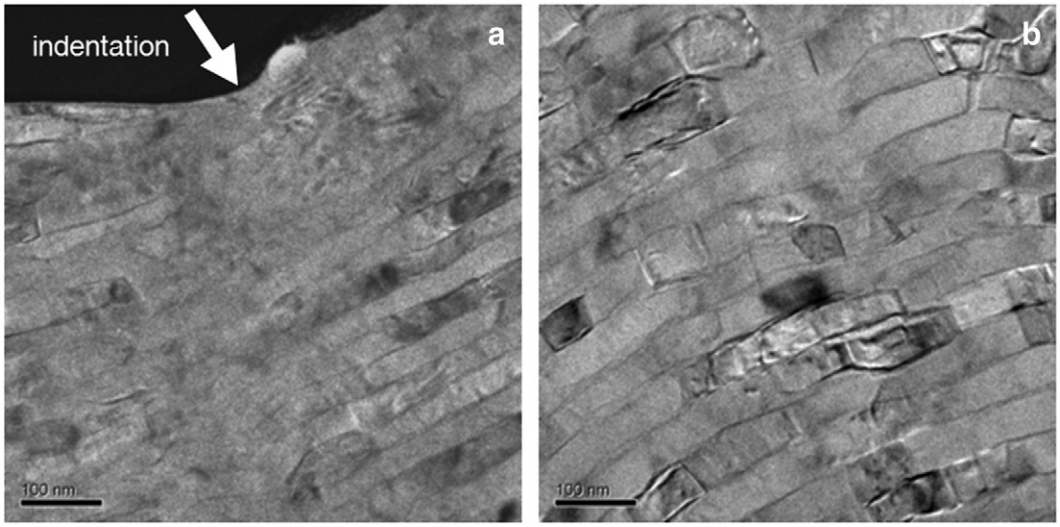

Fig. 5. Indentation cross-section in nanolaminate Al50SiC2 obtained by TEM. (a) General view. (b) Underneath the indented area, but far away from the surface.

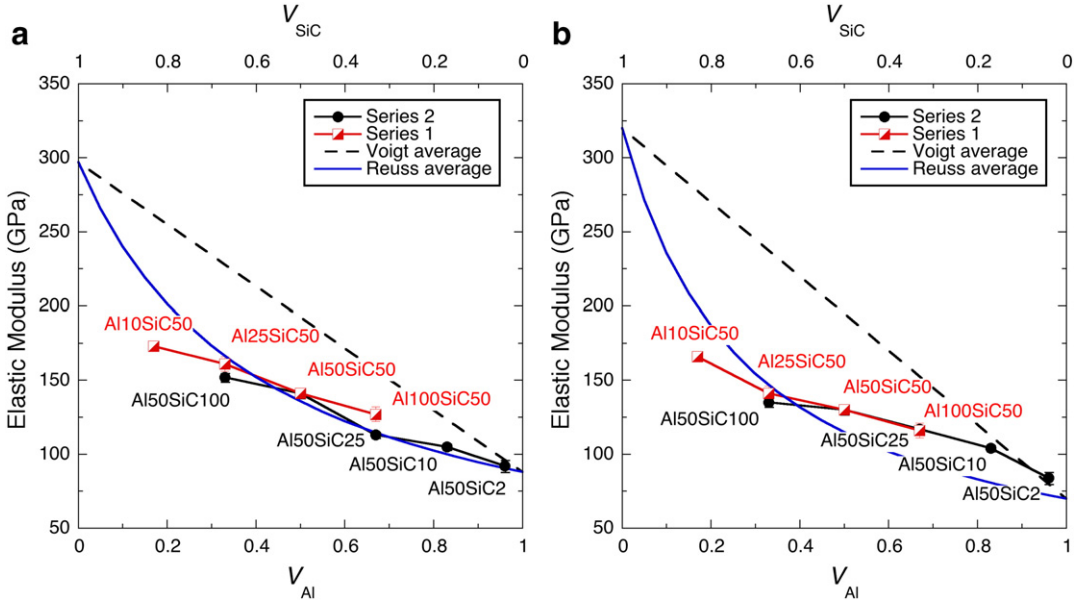

Fig. 6. Elastic modulus of the nanolaminates as a function of Al volume fraction at (a) ambient temperature and (b) 100 °C. The dotted and solid lines represent the Voigt (rule of mixtures) and the Reuss averages (inverse rule of mixtures), respectively.

by the decrease in the flexural modulus of the SiC layers. As such, nanolaminates Al25SiC50 and Al50SiC100, both with $V_{Al} = 0.33$, display the same hardness within experimental error, and so do Al50SiC25 and Al100Si50, both with $V_{Al} = 0.67$, even though the layer thicknesses and the interface densities vary by a factor of 2.

It is also worth noting the difference in hardness between the monolithic Al coating and the Al50SiC2 nanolaminate. Introducing 2 nm thick SiC interlayers between 50 nm thick Al layers increased the hardness from 0.9 GPa for Al up to 3.3 GPa for Al50SiC2. As shown in Fig. 1(b), the thin SiC interlayer interrupts the growth of the columnar grains of Al, forcing the Al layers to re-nucleate on each SiC layer. The impact of this microstructural change on the elastic modulus is negligible, as shown in Fig. 6(a), yet the hardness increased by more than a factor of 3 that has to be attributed to an increase in the yield strength of Al because the thin, SiC layers are not expected to constrain the deformation of the Al layers, as evidenced in Fig. 5. Further increase of the SiC layer thickness in series 2, keeping the Al layer thickness at 50 nm, led to an increase in the hardness, due to the contribution of the constrain imposed by the SiC layers.

In this regard, it is interesting to follow the evolution of the so-called plasticity index, i.e., the ratio H/E, with the volume fraction of Al (and SiC), which is plotted in Fig. 7(b). This plot evidences two different regimes as a function of V_{Al}. The ratio H/E remains constant at roughly 0.4 (compare with $H/E = 0.01$ for monolithic Al coatings) when $V_{Al} > 0.5$, while H/E increases as V_{Al} decreases towards the $H/E = 0.1$ (the ratio corresponding to monolithic SiC) when $V_{Al} < 0.5$. These results seem to indicate that hardness is mainly controlled by the plastic flow of the Al layers and the constraint imposed by the SiC layers when $V_{Al} > 0.5$, so that H and E follow the same trend with V_{Al}. However, H increases more rapidly than E as V_{Al} decreases when $V_{Al} < 0.5$ because the deformation is controlled by the elastic deformation of the SiC layers rather than by the constrained plastic deformation of Al.

The evolution of hardness with temperature depicted in Fig. 8(a) and (b) for series 1 and 2, respectively, can also shed some light on

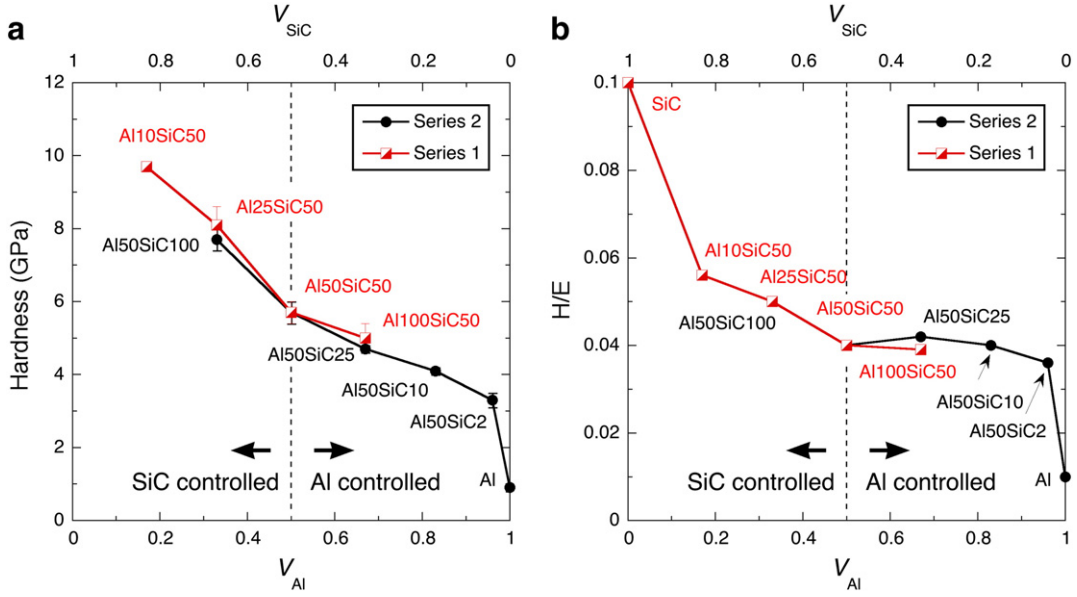

Fig. 7. Influence of Al (and SiC) volume fraction on the room temperature mechanical properties of Al/SiC nanolaminates. (a) Hardness and (b) H/E ratio.

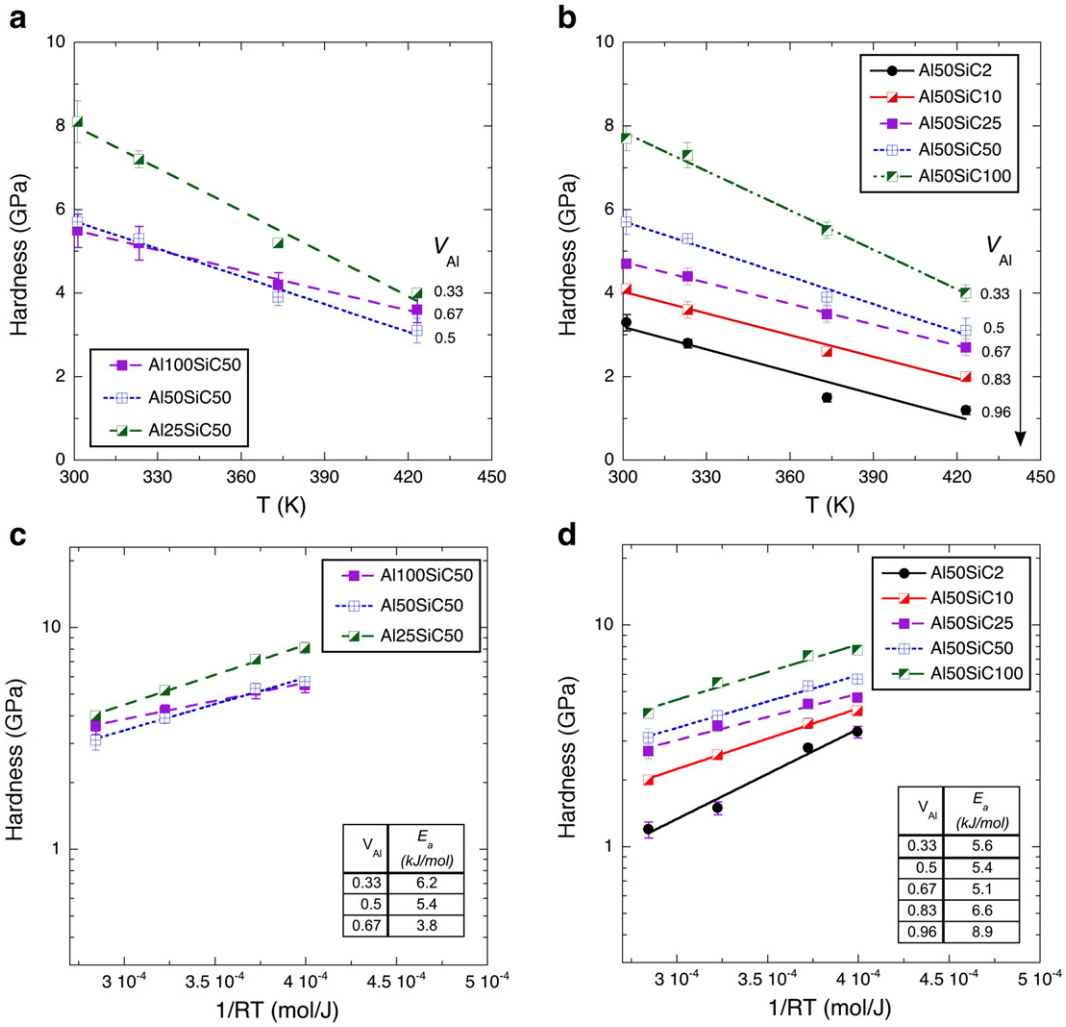

Fig. 8. Evolution of hardness with temperature for Al/SiC nanolaminates. (a) Series 1. (b) Series 2. Graphs (c) and (d) are the corresponding Arrhenius plots to determine the apparent activation energy for hardness.

the dominant deformation mechanisms. There was a marked reduction of the hardness with temperature in all cases but there were some distinctive effects of the layer thickness that were not obvious when at room temperature. In some cases, the influences of the temperature in two nanolaminates were very marked. This is the case of Al50SiC50 and Al100SiC50 in Fig. 8(a). The hardness of the former was 2 GPa higher at room temperature, while the latter became harder at 150 °C.

It is instructive to analyze the influence of the temperature on the hardness using an Arrhenius type equation:

$$H = H_0 exp\left(\frac{E_a}{RT}\right) \tag{3}$$

where H_0 is the extrapolated hardness at 0 K, E_a some apparent activation energy for hardness and R is the universal gas constant. Fig. 8(c) and (d) show the corresponding Arrhenius plot and activation energy of each nanolaminate. In the series 2 of nanolaminates (the Al layer thickness was constant and equal to 50 nm), the variation of the SiC layer thickness between 100 nm and 25 nm had no influence in E_a. This is not surprising because only Al should contribute to the drop in hardness with temperature as SiC is deforming elastically. Only when the SiC layer thickness was reduced below 10 nm, and especially at 2 nm, did the activation energy increased considerably. This can only be explained as a consequence of the increase in interface area, meaning that some interface-mediated deformation mechanism, like interface diffusion or dislocation climbing at the interfaces [39], might become critical processes influencing the strength reduction with temperature. The same trend was observed in the case of series 1, in which excluding nanolaminate Al10SiC50 that presented a large porosity, E_a increased as the Al thickness decreased when the SiC layer thickness was equal to 50 nm. As a consequence, even though Al100SiC50 and Al50SiC25 nanolaminates, both with $V_{Al} = 0.67$, presented the same room temperature hardness, the reduction of hardness with temperature was much higher in the Al50SiC25 nanolaminate because of the higher interface density. Similar results were found for Al50SiC100 and Al25Si50 nanolaminates. They are in agreement with the high temperature micropillar compression studies carried out previously in Al50SiC50 [31], that showed a larger contribution of interface sliding to the deformation as temperature increased from RT to 100 °C.

5. Conclusion

The mechanical properties of Al/SiC nanolaminates as a function of the Al and SiC layer thicknesses (in the range between 2 nm and 100 nm) were measured by means of nanoindentation in the temperature range 28 °C and 150 °C. The elastic modulus of the nanolaminates was in good agreement with the Reuss average (inverse rule-of-mixtures) of the constituents. The room temperature hardness was mainly controlled by the volume fraction of the constituents and independent of the individual Al and SiC layer thicknesses. Since the deformation of the

nanolaminates was controlled by the plastic deformation of the Al layers, constrained by the SiC layers, and by the elastic bending of the SiC layers, this might be due to the fact that the increase in the yield stress of Al with layer thickness reduction might be compensated by the reduction in the flexural modulus of the SiC layers. The hardness of all the nanolaminates decreased rapidly with temperature and the reduction in hardness increased as the layer thickness decreased (higher interface density) for nanolaminates with the same volume fraction of Al and SiC. This behavior was attributed to the activation of deformation mechanisms associated to the interface. This result implies that optimum performance of nanolaminates at high temperature requires a careful design, as evidenced in other nanolaminate systems [5].

Acknowledgements

This investigation was supported by the National Science Foundation of the US and the Spanish Ministry of Economy and Competitiveness under the Materials World Network Program through the project "High temperature mechanical behavior of metal/ceramic nanolaminate composites" (NSF-DMR-1209988 and PCIN-2013-029). The multilayer deposition work at LANL was supported by US DOE, Office of Basic Energy Sciences. Additional support from the Spanish Ministry of Economy and Competitiveness (MAT2012-31889) and the European Commission through the project RADINTERFACES (Grant Agreement Number 263273) is also gratefully acknowledged.

References

[1] D.R. Lesuer, C.K. Syn, O.D. Sherby, J. Wadsworth, J.J. Lewandowski, W.H. Hunt, Mechanical behaviour of laminated metal composites, Int. Mater. Rev. 41 (1996) 169.
[2] N. Mara, A. Sergueeva, A. Misra, A.K. Mukherjee, Structure and high-temperature mechanical behavior relationship in nano-scaled multilayered materials, Scr. Mater. 50 (2004) 803.
[3] A. Misra, J.P. Hirth, R.G. Hoagland, Length-scale-dependent deformation mechanisms in incoherent metallic multilayered composites, Acta Mater. 53 (2005) 4817.
[4] A. Misra, J.P. Hirth, R.G. Hoagland, J.D. Embury, H. Kung, Dislocation mechanisms and symmetric slip in rolled nano-scale metallic multilayers, Acta Mater. 52 (2004) 2387.
[5] M.A. Monclús, S.J. Zheng, J.R. Mayeur, I.J. Beyerlein, N.A. Mara, T. Polcar, et al., Optimum high temperature strength of two-dimensional nanocomposites, APL Mater. 1 (2013) 052103.
[6] M.C. Liu, X.H. Du, I.C. Lin, H.J. Pei, J.C. Huang, Superplastic-like deformation in metallic amorphous/crystalline nanolayered micropillars, Intermetallics 30 (2012) 30.
[7] X. Deng, N. Chawla, K.K. Chawla, M. Koopman, J.P. Chu, Mechanical Behavior of Multilayered Nanoscale Metal–ceramic Composites, Adv. Eng. Mater. 7 (2005) 1099.
[8] X. Deng, C. Cleveland, N. Chawla, T. Karcher, M. Koopman, K.K. Chawla, Nanoindentation behavior of nanolayered metal–ceramic composites, J. Mater. Eng. Perform. 14 (08/01/2005) 417.
[9] I. Knorr, N.M. Cordero, E.T. Lilleodden, C.A. Volkert, Mechanical behavior of nanoscale Cu/PdSi multilayers, Acta Mater. 61 (2013) 4984.
[10] H.C. Barshilia, M.S. Prakash, A. Jain, K.S. Rajam, Structure, hardness and thermal stability of TiAlN and nanolayered TiAlN/CrN multilayer films, Vacuum 77 (2005) 169.
[11] H.C. Barshilia, M. Surya Prakash, A. Poojari, K.S. Rajam, Corrosion behavior of nanolayered TiN/NbN multilayer coatings prepared by reactive direct current magnetron sputtering process, Thin Solid Films 460 (2004) 133.
[12] S.J. Lloyd, J.M. Molina-Aldareguia, W.J. Clegg, Structural characterization of TiN/NbN multilayers: X-ray diffraction, energy-filtered TEM and Fresnel contrast techniques compared, J. Microsc. 217 (2005) 241.
[13] J.M. Molina-Aldareguia, S.J. Lloyd, M. Odén, T. Joelsson, L. Hultman, W.J. Clegg, Deformation structures under indentations in TiN/NbN single-crystal multilayers deposited by magnetron sputtering at different bombarding ion energies, Philos. Mag. A 82 (2002) 1983.
[14] D.A. Chance, D.L. Wilcox, Metal–ceramic constraints for multilayer electronic packages, Proc. IEEE 59 (1971) 1455.
[15] F. Jiménez-Villacorta, A. Espinosa, E. Céspedes, C. Prieto, Magnetic properties and short-range structure analysis of granular cobalt silicon nitride multilayers, J. Appl. Phys. 110 (2011) (pp).
[16] A. García-García, A. Vovk, J.A. Pardo, P. Štrichovanec, C. Magén, E. Snoeck, et al., Magnetic properties of Fe/MgO granular multilayers prepared by pulsed laser deposition, J. Appl. Phys. 105 (2009) (pp).
[17] O. Lenoble, P. Bauer, J.F. Bobo, H. Fischer, M.F. Ravet, M. Piecuch, Thermal behaviour and magnetic properties of Fe/Al 2 O 3 multilayers, J. Phys. Condens. Matter 6 (1994) 3337.
[18] C. Nunes, V. Teixeira, M.L. Prates, N.P. Barradas, A.D. Sequeira, Graded selective coatings based on chromium and titanium oxynitride, Thin Solid Films 442 (2003) 173.
[19] Z. Qi-Chu, Optimizing analysis of W-AlN cermet solar absorbing coatings, J. Phys. D. Appl. Phys. 34 (2001) 3113.
[20] H. Holleck, V. Schier, Multilayer PVD coatings for wear protection, Surf. Coat. Technol. 76–77 (1995) 328 (Part 1).
[21] S. PalDey, S.C. Deevi, Single layer and multilayer wear resistant coatings of (Ti, Al)N: a review, Mater. Sci. Eng. A Struct. Mater. Prop. Microstruct. Process. 342 (Feb 2003) 58.
[22] J.C. Trenkle, C.E. Packard, C.A. Schuh, Hot nanoindentation in inert environments, Rev. Sci. Instrum. 81 (2010) 073901.
[23] J.M. Wheeler, J. Michler, Elevated temperature, nano-mechanical testing in situ in the scanning electron microscope, Rev. Sci. Instrum. 84 (2013) 045103.
[24] J.F. Smith, S. Zheng, High temperature nanoscale mechanical property measurements, Surf. Eng. 16 (2000) 143.
[25] S. Lotfian, Mechanical Characterization of Lead-Free Sn-Ag-Cu Solder Joints by High-Temperature Nanoindentation, J. Electron. Mater. 42 (2013) 1085.
[26] S. Lotfian, J.M. Molina-Aldareguia, K.E. Yazzie, J. Llorca, N. Chawla, High-temperature nanoindentation behavior of Al/SiC multilayers, Philos. Mag. Lett. 92 (2012) 362.
[27] G. Tang, Y.L. Shen, D.R.P. Singh, N. Chawla, Analysis of indentation-derived effective elastic modulus of metal–ceramic multilayers, Int. J. Mech. Mater. Des. 4 (2008) 391.
[28] G. Tang, Y.L. Shen, D.R.P. Singh, N. Chawla, Indentation behavior of metal–ceramic multilayers at the nanoscale: Numerical analysis and experimental verification, Acta Mater. 58 (Apr 2010) 2033.
[29] G. Tang, Y.L. Shen, N. Chawla, Plastic deformation during indentation unloading in multilayered materials, J. Appl. Phys. 104 (2008) 116102.
[30] D.R.P. Singh, N. Chawla, G. Tang, Y.L. Shen, Micropillar compression of Al/SiC nanolaminates, Acta Mater. 58 (2010) 6628.
[31] S. Lotfian, M. Rodríguez, K.E. Yazzie, N. Chawla, J. Llorca, J.M. Molina-Aldareguía, High temperature micropillar compression of Al/SiC nanolaminates, Acta Mater. 61 (2013) 4439.
[32] W.C. Oliver, G.M. Pharr, An improved technique for determining hardness and elastic modulus using load and displacement sensing indentation experiments, J. Mater. Res. 7 (1992) 1564.
[33] L.L. Snead, T. Nozawa, Y. Katoh, T.-S. Byun, S. Kondo, D.A. Petti, Handbook of SiC properties for fuel performance modeling, J. Nucl. Mater. 371 (2007) 329.
[34] N. Chawla, D.R.P. Singh, Y.L. Shen, G. Tang, K.K. Chawla, Indentation mechanics and fracture behavior of metal/ceramic nanolaminate composites, J. Mater. Sci. 43 (07/01/2008) 4383.
[35] D.R.P. Singh, N. Chawla, Y.L. Shen, Focused Ion Beam (FIB) tomography of nanoindentation damage in nanoscale metal/ceramic multilayers, Mater. Charact. 61 (Apr 2010) 481.
[36] D. Bhattacharyya, N.A. Mara, P. Dickerson, R.G. Hoagland, A. Misra, Compressive flow behavior of Al–TiN multilayers at nanometer scale layer thickness, Acta Mater. 59 (2011) 3804.
[37] D. Bhattacharyya, N.A. Mara, P. Dickerson, R.G. Hoagland, A. Misra, A transmission electron microscopy study of the deformation behavior underneath nanoindents in nanoscale Al–TiN multilayered composites, Philos. Mag. 90 (05/07/2010) 1711.
[38] M.A. Monclus, S. Lotfian, J.M. Molina-Aldareguia, Tip shape effect on the hot indentation hardness and modulus of Al and SiC coatings, Int. J. Precis. Eng. Manuf. (2014) (to be published).
[39] J. Wang, R.G. Hoagland, A. Misra, Room-temperature dislocation climb in metallic interfaces, Appl. Phys. Lett. 94 (2009) 131910.